Location and extent of the subducted Chile Ridge from Rayleigh wave phase velocities

Simon Lloyd[1,3], Suzan van der Lee[1], and Ray Russo[2]

We cross-correlate fundamental mode Rayleigh waves recorded at different seismic stations of the Chile Ridge Subduction Project in southern Chile in order to obtain the relative propagation time to each station. Using these relative times we image the wave front as it passes through the array and observe effects of lateral heterogeneity both inside and outside the array region. Previously performed body wave tomography imaged a low-velocity slab window at the expected location of the subducted Chile Ridge. We subdivide the stations into different groups and infer Rayleigh wave phase velocities at different periods for each group. The resulting dispersion curves are then inverted for S-velocity depth profiles, to constrain the vertical extent of the slab window. We find evidence for the top of the slab window to lie at 50 km depth. Resolution tests with synthetic data suggest the bottom of the slab window lies at 150 km depth.

1. Introduction

At the triple junction between the Nazca, South American, and Antarctic plates the Chile ridge is being subducted beneath South America [*Cande and Leslie*, 1987; *Breitsprecher and Thorkelson*, 2009]. Because the Nazca and Antarctic plates have a diverging component in their relative plate motion, the subducted spreading center widens with distance from the trench. Once subducted no new lithosphere is formed, but the trailing edge of the Antarctic plate separates progressively at $\sim$5 cm/yr from the leading edge of the Nazca plate, opening a slab window. Such a window allows asthenospheric mantle to flow between the two slabs, effecting mantle chemistry and thermal regime, seismic velocities and anisotropy as well as surface geology [*Russo et al.*, 2010]. We use surface wave dispersion recorded at the seismometers of the Chile Ridge Subduction Project (CRSP) to seismically constrain the slab window.

Typically, one or two station methods have been used to calculate the average phase velocity along the surface wave propagation path. With the emergence of densely spaced seismic arrays, methods involving multiple stations have been successfully employed e.g. in southern Germany [*Friedrich*, 1998], northern California [*Pollitz*, 1999], in the oceanic MELT array [*Forsyth and Li*, 2005],

[1]Department of Earth and Planetary Sciences, Northwestern University, Evanston, Illinois, USA

[2]Department of Geological Sciences, University of Florida, Gainesville, Florida, USA

[3]Now at Department of Meteorology and Geophysics, University of Vienna, Austria

0094-8276/11/$5.00

and more recently in the western United States using the EarthScope array [*Lin et al.*, 2009]. Unlike single path methods, the array methods account for off-great circle wave paths and the resulting non–planar wave fronts [*Friederich et al.*, 1998], thus eliminating a potential bias when calculating *S*-velocities.

The CRSP stations also form an array, consisting of 39 Broadband seismic stations deployed to investigate seismic structure of the subducting Chile Ridge. Using body waves, an asthenosphere-filled gap was tomographically imaged and mantle flow direction was inferred from shear wave splitting [*Russo et al.*, 2010]. Using Rayleigh wave forms, we investigate regional velocity structure depths and depth extent of the slab window. Owing to the small inter-station distance within the CRSP array, we can image Rayleigh wave fronts as they pass through the array and infer *S*-velocity structure from the shape of these wave fronts [e.g. *Wielandt*, 1993]. The wave fronts (or phase fronts) are obtained from cross correlating the wave forms and then contouring the relative travel times to different stations. Interpolation of these travel times on a regular grid and calculation of the spatial gradient provides a direct measurement of phase slowness and thus velocity [*Lin et al.*, 2009]. However, since the CRSP array is substantially smaller than the EarthScope transportable array used by *Lin et al.* [2009] and because we posses *a priori* knowledge of the slab window location from *Russo et al.* [2010], we propose a different method, which is to calculate average phase velocities directly from the relative travel times for selected groups of stations within a particular region, without prior interpolation.

2. Method

We make use of the fact that because CRSP interstation distances are small, the recorded seismograms are similar from station to station. Our goal is to determine the relative travel times of incoming Rayleigh waves by cross-correlating seismograms recorded at different stations. We then use these times to image the Rayleigh wave front as it passes through the array and to investigate the velocity structure in the upper mantle.

We use only the fundamental mode Rayleigh wave because it can be cleanly isolated from other modes and phases. We prepare the data by removing higher mode Rayleigh waves and noise using phase matched filtering [e.g. *Herrin and Goforth*, 1977]. We apply a Gaussian filter centered at a range of periods (20 – 80 s) and cross-correlate all seismograms with each other. The optimum relative travel times for all stations are determined in a least squares procedure analogous to that of *VanDecar and Crosson* [1990]. The station at which the wave front arrives first is assigned a time of 0 s, and all other times for that event are relative to the time at that station. Plotting these values on a map and contouring them represents snapshots of the Rayleigh wave front as it passes through the array (Fig. 1). The shapes of these contours are indicative of phase velocity perturbations both inside and outside of the array, and the slope of the contours is essentially the inverse phase velocity inside the array region. However, the average phase velocity for the array region is easily obtained directly from the relative arrival times. We calculate it first assuming the wave front is always perpendicular to the great circle path connecting the stations with the earthquake source location. As we find that assumption is typically not correct we then compute best fitting off great circle paths for the incoming waves for our phase velocity calculation. This compensates for effects on the arrival time that occurred outside the array region. These calculations can be performed with an arbitrary number of stations greater than four. We therefore split the stations into different groups. First, we group them by dividing the stations using lines of constant latitude and longitude, to obtain independent estimates of phase velocities, and then we use *a priori* knowledge to select stations for two groups depending on whether they sit on top of the slab or the window as outlined by body waves [*Russo et al.*, 2010, Fig. 3]. Finally, we obtain phase velocities for the different periods in the two regions (i.e. dispersion curves) which we then invert for S-velocity depth profiles ($\beta(z)$).

3. Wave fronts

After determining relative arrival times of the Rayleigh waves from cross-correlating the seismograms, we interpolate the times on to a regular grid and plot contours every 10 seconds. The number of stations we use varies for each event and period, depending on the total number of active stations and the quality of the signal at a particular period. Fig. 1 shows how the Rayleigh wave front of a teleseismic event located off the western margin of Mexico propagates through the array. In this example, the shape of the wave front appears relatively planar. Inferring seismic structure beneath the array from the shape of the contours (i.e. bending of the otherwise planar contours due to lateral heterogeneity) directly is therefore difficult. We can, however, observe effects due to lateral heterogeneity outside the array region before the wave front reaches the array; for events such as the one shown, with wave fronts arriving roughly perpendicular to the western margin of South America, the wave fronts are generally not perpendicular the the great circle path connecting each station with the epicenter. At longer periods the effect becomes negligible, and thus we attribute it to the crust and mantle just below the crust, as shorter periods (20-35 s) are more sensitive to structure at these depths. The wave front arrives earlier at western stations than eastern ones, most likely due to the differences between the oceanic lithosphere of the Nazca plate to the west and the continental South American plate in the east. Because of the thinner crust in oceanic lithosphere compared to continental lithosphere, surface waves traveling through oceans are sensitive to a larger portion of the mantle just beneath the crust. This increases their velocities relative to continental lithosphere and explains our observation in Fig. 1. While important, the nature of these observations is qualitative only. To infer seismic structure beneath the array, we base our calculations on the measured arrival times directly, without interpolating them on to a grid first.

4. *S*-velocity structure beneath the CRSP array

We first estimate the average Rayleigh wave phase velocity over the entire array region. We define a relative distance as the distance along the great circle path connecting the earthquake epicenter with the receivers minus the epicentral distance of the station nearest to the epicenter. Using the relative travel times from the cross-correlation together with the relative distances, we calculate an average Rayleigh wave phase velocity for the entire array region. Multiplying the best fitting velocity with the relative great circle travel distance gives us a calculated (relative) travel time, which we compare with the observed travel time. Typically the calculated travel time does not match the observed travel time very well (Fig. 2a). This could be due to heterogeneity within the array or perhaps the relative distances are incorrect. The Rayleigh waves typically do not arrive exactly along the great circle and their wave fronts may be deformed by structure outside the array. Thus the actual relative distances are indeed not the ones used above and need to be calculated more carefully. Our focus is on the velocity structure within the array, which is why we compensate for the off great circle paths by allowing the earthquake source to move (in both space and time) when calculating average phase velocity. It is not actually possible to relocate the earthquake hypocenter using the long-traveled long period Rayleigh waves at our disposal. However, we can estimate the effects of source misslocation using an objective function

$$e = \sum_{i=1}^{N} s\Delta_i(\lambda_0, \theta_0) - s\Delta_1(\lambda_0, \theta_0) - \delta t_i, \qquad (1)$$

to account for effects of structure outside the CRSP array on the observed wave fronts. Δ_i is the great circle distance from the ith station to a hypothetical source (λ_0, θ_0), s is slowness (inverse of Rayleigh phase velocity), and N is the number of stations. Note that $i = 1$ is defined to be the station with 0 sec observed relative travel time. We solve this equation numerically using the Levenberg–Marquardt algorithm [*Marquardt*, 1963] to obtain a refined estimate on average Rayleigh wave phase velocity in the array region. The hypothetical new source which is also obtained simply compensates for path effects outside the array. We compare the inferred travel time with our observations, and find that the new method yields a better fit (Fig 2b). This improvement indicates that the poor match in Fig. 2a is primarily due to lateral heterogeneity affecting the incoming wave front before it reaches the CRSP array.

In order to compare different sub-regions within the array, we first split the stations into two groups along the 73°W meridian. At longer periods (e.g. 60 seconds), we find a negligible difference in velocity between the east and the west. However, at shorter periods such as ∼30 seconds we obtain slower velocities in the eastern, more continental section of the array compared to the west, which is more oceanic (Fig. 3a, b). The phase velocity sensitivity of a 30 second period Rayleigh wave to shear velocity structure is greatest in the crust and sub-Moho mantle. It is therefore likely that the velocity difference is due to a shallower Moho on the western side of the Andean crustal root. This also explains the bending of the wave fronts at these periods as they traverse the array (Fig. 1).

The lateral extent of the slab window has been imaged by body waves [*Russo et al.*, 2010]. Here, we provide depth constraints on the window using Rayleigh waves. We divide the stations into two groups: one with stations beneath which there is slab according to the body wave tomography; the other group contains stations above the window. For both groups we invert the relative travel times by minimizing the objective function (1). We do this for several events and get estimates of phase velocity in the two regions. At a period of 60 seconds we consistently observe lower velocities in the slab window (Fig.

3c, d). Performing this analysis for several periods we obtain phase velocity dispersion curves for the two station groups (Fig. 4a). We invert the dispersion curves for S-velocity depth profiles using the 1D background model CR35, which we derive from the model MC35 [*Van der Lee and Nolet*, 1997] by adjusting P- and S-velocities so that the calculated Rayleigh wave phase velocities lie between measured phase velocities of slab and window. CR35 is then used to calculate group velocity sensitivity to S-velocity perturbations ($\Delta\beta(z)$), which allows obtaining S-velocity profiles by inverting a linear system. The profiles for velocity structure beneath the two regions are similar in the crust and down to 50 km depth in the mantle (Fig. 4b). They then diverge with increasing depth until a maximum difference between them is reached at 70-100 km, after which they gradually start converging again until they become identical below about 250 km (Fig 4c).

Examining sensitivity kernels of fundamental mode Rayleigh waves at the periods used in this study, we expect good resolution down to at least 100 km depth. We interpret velocity divergence in the two models beginning at 50 km depth as the bottom of the lithosphere of the overriding South American plate and the top of the subducting slab and asthenosphere filled slab window, respectively. Conversely, at depths greater than 150 km the resolving power of fundamental mode Rayleigh waves diminishes and introduces ambiguity in the likely location of the bottom of slab window region. There is no clear similarly rapid increase or decrease in velocity as observed at 50 km depth. We investigate the resolving power of our data using different hypothetical slab windows (i.e. pairs of models for slab or slab window regions). Fig. 5. shows 3 hypothetical slab windows, which all have the top at 50 km depth but end at increasing depths. We calculate phase velocities for these models and invert them analogously to the observed phase velocities and compare the resulting retrieved S-velocity models with the respective input models, as well as the measured S-velocity model difference (Fig. 4c). We find that the observed velocity difference can be matched well using a simple box model ranging from 50 km to 150 km (Fig. 5b). Decreasing (Fig. 5a) or increasing (Fig. 5c) the depth extent of the slab window changes the shape of our retrieved model. If the slab window depth extent is small we retrieve velocity differences which are too high at shallow depths and too low at greater depths, and if the depth extent is too large, we find the converse. Thus, we may infer that the true depth extent of the slab is similar to the hypothetical model in Fig. 5b, which places the top at the strongest velocity difference jump and the bottom at the depth where the difference becomes less than 50% of the maximum amplitude, i.e. roughly 150 km.

5. Conclusions

Small distances between the stations in the CRSP array result in recorded surface waves that are relatively similar at all stations. We cross-correlate the wave forms and determine relative travel times to different stations. Fitting wave fronts to these travel times shows how the array region is traversed and illustrates the effects of lateral heterogeneity both inside and outside the array region. Experimentation reveals that the strongest heterogeneity recorded by the Rayleigh waves is indeed related to the contrast between the region of the slab window and the region without.

We refine our definition of the slab window region using results from body wave tomography [*Russo et al.*, 2010] to divide the array in two groups. For each group we determine Rayleigh wave phase velocities at different periods ranging from 25 to 80 seconds to obtain a dispersion curve, which we invert for S-velocity depth profiles. The differences between the two profiles highlight the vertical extent of the slab window. The window affects S-velocity starting beneath the thin lithosphere of the overriding plate at 50 km depth, with a peak in sensitivity at ∼130 km depth. After that it tapers off, reduced by about two thirds at 200 km. The top of the slab window is constrained by a strong change in velocity difference between slab and slab window regions. No such change is seen for the bottom of the slab window. In order to determine the bottom of the slab window we perform resolution tests with synthetic models, which suggest it lies near 150 km depth.

Acknowledgments. We are very grateful to Diana Comte of the University of Chile, Santiago; Victor Mocanu of the University of Bucharest, Alejandro Gallego, University of Hawaii; Ruth Murdie, Goldfields Australia, and John VanDecar, DTM-Carnegie, for their work in collecting the CRSP data. This work was supported by U.S. National Science Foundation grant EAR-0538267. The Chile Ridge Subduction Project was supported by U.S. National Science Foundation grant EAR-0126244 to R. Russo, and CONICYT-Chile grant 1050367 to D. Comte.

References

Breitsprecher, K., and K. Thorkelson (2009), Neogene kinematic history of the nazca-antarctic-phoenix slab windows beneath patagonia and the antarctic peninsula, *Tectonophys.*, *464*, 10–20, doi:10.1016/j.tecto.2008.02.013.

Cande, S., and R. Leslie (1987), Late cenozoic tectonics of the southern chile trench, *J. Geophys. Res.*, *91*, 495–520, doi:10.1029/JB091iB01p00471.

Forsyth, D., and A. Li (2005), Array analysis of two-dimensional variations in surface wave phase velocity and azimuthal anisotropy in the presence of multipathing interference, in *Seismic Earth: Array Analysis of Broadband Seismograms*, p. 8197, AGU.

Friederich, W., E. Wielandt, and S. Stange (1998), Nonplane geometries of seismic surface wavefields and their implications for regional surfacewave tomography, *Geophys. J. Int*, *132*, 203225.

Friedrich, W. (1998), Wavetheoretical inversion of teleseismic surface waves in a regional network: Phase velocity maps and a three-dimensional upper-mantle shear-wave velocity model for southern Germany, *Geophys. J. Int.*, *132*, 203225.

Herrin, E., and T. Goforth (1977), Phase-matched filters; application to the study of rayleigh waves, *Bull. Seismol. Soc. Am.*, *67*(5), 12591275.

Lin, F., M. Ritzwoller, and R. Snieder (2009), Eikonal tomography: surface wave tomography by phase front tracking a regional broad-band seismic array, *Geophys. J. Int.*, *177*, 10911110.

Marquardt, D. W. (1963), An algorithm for least-squares estimation of nonlinear parameters, *SIAM Journal on Applied Mathematics*, *11*(2), 431441, doi:10.1137/0111030.

Pollitz, F. (1999), Regional velocity structure in northern california from inversion of scattered seismic surface waves,, *J. geophys. Res.*, *104*, 15,04315,072.

Russo, R., J. C. VanDecar, D. Comte, A. Gallego, and R. E. Murdie (2010), Subduction of the chile ridge: Upper mantle structure and flow, *GSA Today*, *20*(9).

Van der Lee, S., and G. Nolet (1997), Upper Mantle S-Velocity Structure of North America, *J. of Geophys. Res.*, *102*, 22,81522,838.

VanDecar, J. C., and R. S. Crosson (1990), Determination of teleseismic relative phase arrival times using multi-channel cross-correlation and least squares, *Bull. Seismol. Soc. Am.*, *80*(1), 150169.

Wielandt, E. (1993), Propagation and structural interpretation of non-plane waves, *Geophys. J. Int.*, *113*, 4553.

Suzan van der Lee, Department of Earth and Planetary Sciences, Northwestern University, 1850 Campus Drive, Evanston, IL 60208-2150, USA (suzan@earth.northwestern.edu)

Simon M. Lloyd, Department Meteorology and Geophysics, University of Vienna, UZA II, Althanstrasse 14, Vienna, 1090, Austria (simon.lloyd@univie.ac.at)

Raymond M. Russo, Department of Geological Sciences, University of Florida, 223 Williamson Hall, PO Box 112120, Gainesville, Florida USA (rrusso@ufl.edu)

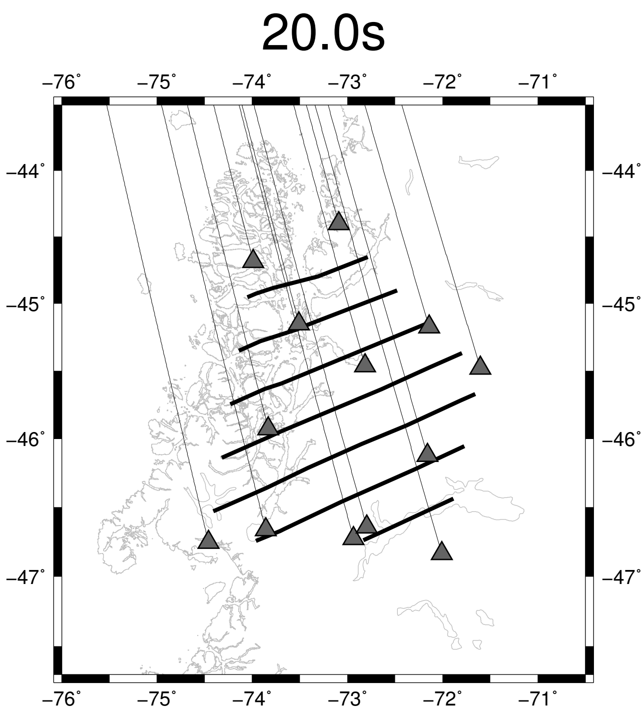

Figure 1. 10 second interval contour lines after interpolating relative arrival times of Rayleigh waves at selected CRSP stations. Small non-planar features indicate lateral inhomogeneity within the array region. The contour lines are non-perpendicular to the great circle paths connecting stations and event, caused by inhomogeneity outside the array region.

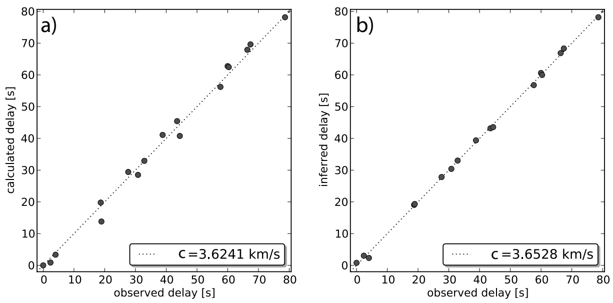

Figure 2. a) Using the measured relative arrival times together with the relative great circle distance we calculate average Rayleigh wave phase velocity for the array region. The resulting model inadequately predicts observed delay due to the real wave paths entering the array at angles that are different from the great circle paths. b) Correcting for off great circle paths yields a superior model.

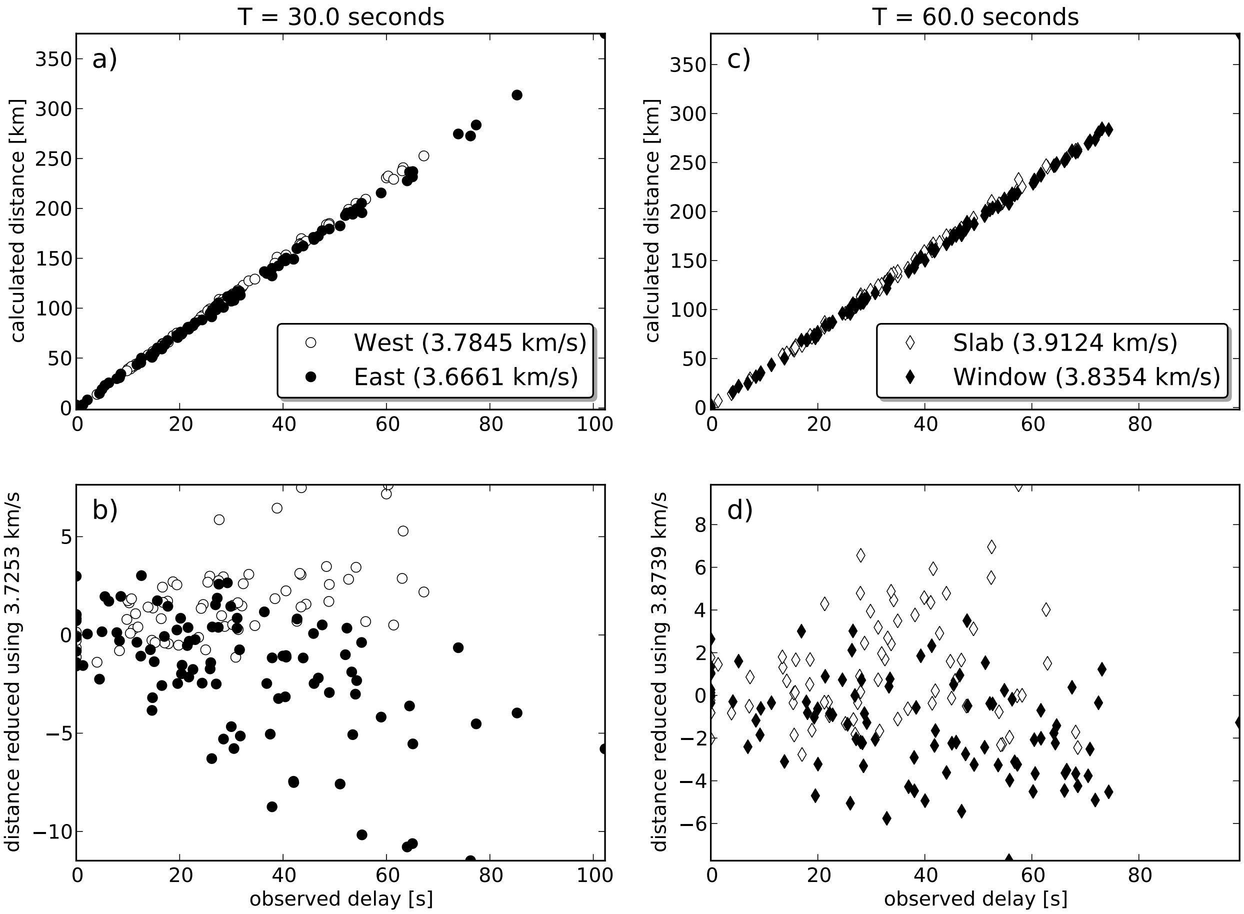

Figure 3. a) We divide the array in two subregions, West and East, and compare average Rayleigh wave phase velocities at 30 s period. The velocities in the W are higher than in the E, which we attribute to differences in oceanic vs continental lithosphere. b) Same as (a), but with a reduced distance to display the different velocities more clearly. c) Dividing the array into to groups using *a priori* knowledge of the slab window location we find slower phase velocities at 60 s period in the slab window region. d) same as (c), but with reduced distance.

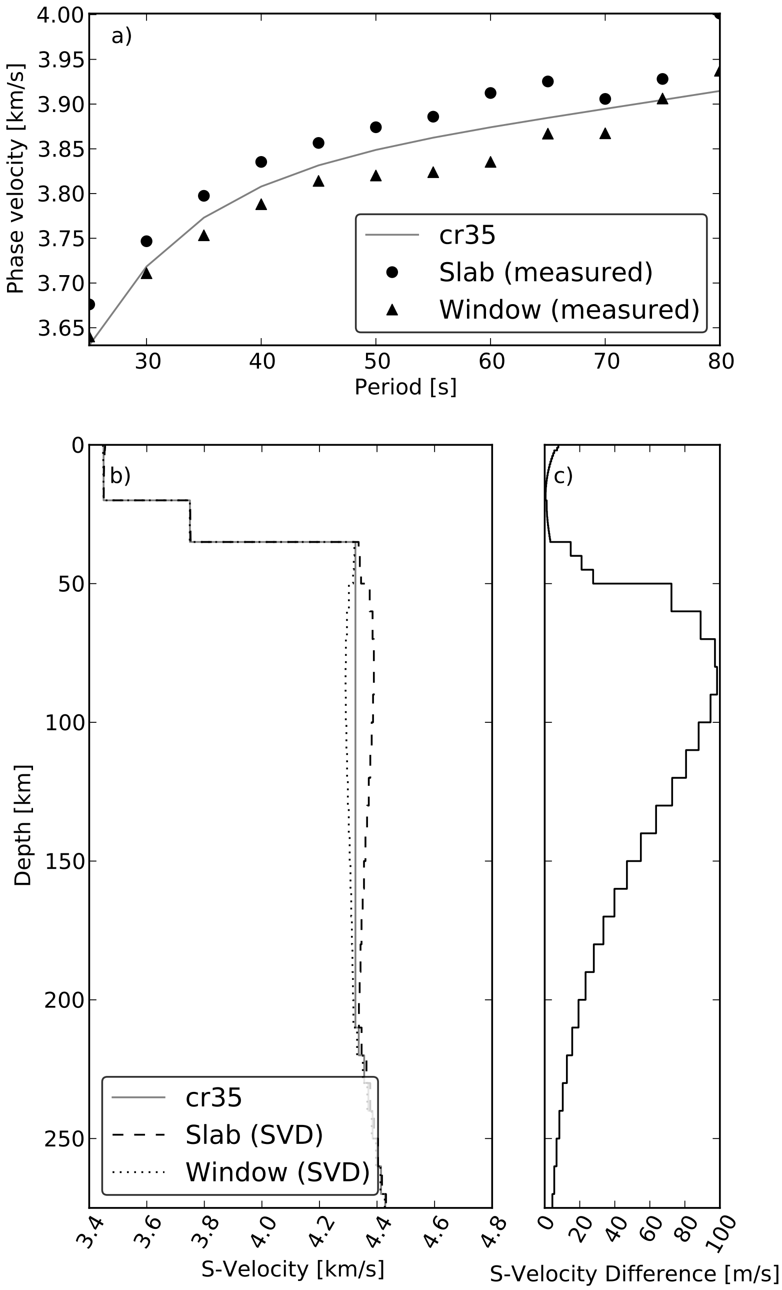

Figure 4. a) Measured Rayleigh wave phase velocities for the two station groups (slab or slab window). The solid line is the calculated phase velocity of the background model CR35. b) Inverted S-velocity depth profiles of the two regions. c) Difference between the velocity profiles of the slab and slab window regions.

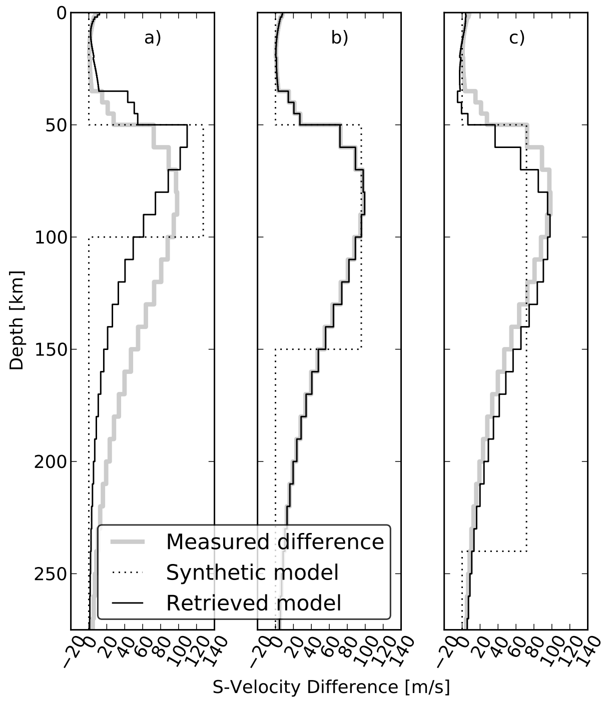

Figure 5. Resolution test with synthetic input models with slabs of different depth extents to calculate phase velocities for inversion. The gray line is the measured difference (Fig. 4c), the dotted line is our input model and the solid line is the recovered model after inverting the synthetic data.